Nano Energy 75 (2020) 104916

Contents lists available at ScienceDirect

Nano Energy

journal homepage: http://www.elsevier.com/locate/nanoen

Quantum prediction of ultra-low thermal conductivity in lithium intercalation materials

Tianli Feng [a,b,c,**], Andrew O'Hara [a], Sokrates T. Pantelides [a,b,d,*]

[a] Department of Physics and Astronomy, Vanderbilt University, Nashville, TN, 37235, USA
[b] Center for Nanophase Materials Sciences, Oak Ridge National Laboratory, Oak Ridge, TN, 37831, USA
[c] Energy and Transportation Science Division, Oak Ridge National Laboratory, Oak Ridge, Tennessee 37831, USA
[d] Department of Electrical Engineering and Computer Science, Vanderbilt University, Nashville, TN, 37235, USA

ARTICLE INFO

Keywords:
Lithium intercalation materials
Batteries
Thermal conductivity
First principles
Four-phonon scattering

ABSTRACT

Lithium-intercalated layered transition-metal oxides, Li_xTMO_2, brought about a paradigm change in rechargeable batteries in recent decades and show promise for use in memristors, a type of device for future neural computing and on-chip storage. Thermal transport properties, although being a crucial element in limiting the charging/discharging rate, package density, energy efficiency, and safety of batteries as well as the controllability and energy consumption of memristors, are poorly managed or even understood yet. Here, for the first time, we employ quantum calculations including high-order lattice anharmonicity and find that the thermal conductivity κ of Li_xTMO_2 materials is significantly lower than hitherto believed. More specifically, the theoretical upper limit of κ of $LiCoO_2$ is 6 W/m-K, 2–6 times lower than the prior theoretical predictions. Delithiation further reduces κ by 40–70% for $LiCoO_2$ and $LiNbO_2$. Grain boundaries, strain, and porosity are yet additional causes of thermal-conductivity reduction, while Li-ion diffusion and electrical transport are found to have only a minor effect on phonon thermal transport. The results elucidate several long-standing issues regarding the thermal transport in lithium-intercalated materials and provide guidance toward designing high-energy-density batteries and controllable memristors.

1. Introduction

The discovery of layered lithium transition-metal oxides ($LiTMO_2$), especially $LiCoO_2$, had a major impact on rechargeable batteries in the past few decades [1,2]. $LiTMO_2$ stores lithium ions between TMO_2 layers with extraordinary mobility, energy density, power density, stability, and long cycle life. $LiTMO_2$-based Li^+-ion batteries are now widely used in most portable electronic devices [3–7]. Recently, the family of $LiTMO_2$ materials, including $LiCoO_2$ and $LiNbO_2$, were also found to be promising candidates for memristors [8–11], a type of device that can retain internal resistance based on the history of applied voltage and current, with potential for neural computing and on-chip storage [12–14]. However, it was realized in recent years that boosting the performance of batteries and memristors is not a trivial task because performance is determined by many coupled properties [3,4,15–18]. Thermal transport properties are a crucial element in this mix as it limits the charging/discharging rate, package density, energy efficiency, and safety of batteries in many applications, especially electric vehicles [19–23]. The ultra-low thermal conductivity [24] of $LiCoO_2$ is the largest drawback that contrasts sharply with other extraordinary electrical and chemical properties for battery applications. In particular, the recently identified localized hotspots [25] push the thermal issue from outside to inside the $LiCoO_2$ electrodes. Thermal transport plays a major role in the operation of memristors as well, since the on/off states are switched via ionic movements driven by nanoscale Joule heat [8–11]. Ultra-low thermal conductivity is necessary to confine the Joule heat for the realization of in-memory computing with low energy consumption.

Despite their significance in various applications, the thermal transport properties of $LiTMO_2$ have not been adequately explored or understood compared to electrical and ionic transport properties, due to limitations of theoretical and experimental capabilities. Theoretically, the evaluation of high-order lattice anharmonicity and phonon

* Corresponding author. Department of Physics and Astronomy and Department of Electrical Engineering and Computer Science, Vanderbilt University, Nashville, TN, 37235, USA.
** Corresponding author. Energy and Transportation Science Division, Oak Ridge National Laboratory, Oak Ridge, Tennessee 37831, USA.
E-mail addresses: fengt@ornl.gov (T. Feng), pantelides@vanderbilt.edu (S.T. Pantelides).

https://doi.org/10.1016/j.nanoen.2020.104916
Received 23 January 2020; Received in revised form 16 April 2020; Accepted 30 April 2020
Available online 23 May 2020

scattering by parameter-free quantum calculations has until recently [26–28] been inaccessible. Available theoretical studies have been based on either classical molecular dynamics [29] or lowest-order anharmonicity [30], which lack sufficient predictive power. As shown in Ref. [31], high-order lattice anharmonicity can induce high-order phonon-phonon scattering, which provides additional phonon-scattering channels and increases the total phonon scattering rates or, equivalently, reduces the phonon relaxation times and thermal conductivity. It was shown that high-order phonon-phonon scattering is generally important for low thermal conductivity materials, complex crystals with many phonon branches, materials with ionic Coulombic interactions, and most materials at high temperatures. At the same time, experimental work has been limited to polycrystals [24]. Overall, the available theoretical and experimental works have not provided deep physical insights into the underlying quantum mechanisms. As a result, several fundamental yet practically significant questions have remained open:

(1) What are the intrinsic (anisotropic) thermal conductivities of Li_xTMO_2?
(2) What is the impact of charging on the vibrational properties and thermal conductivity of Li_xTMO_2 ($x \leq 1$)?
(3) As most practical devices are made using polycrystals, how strongly does the grain size affect the thermal conductivity of Li_xTMO_2 polycrystals? How much can we tune the thermal conductivity by tuning the grain size via tuning the annealing temperature?
(4) As large internal strains are usually generated during charging/discharging cycles, what is the impact of strain on the thermal transport?
(5) As lithium atoms are mobile, making Li_xTMO_2 half-solid half-liquid-like, what is the impact of Li liquidity on the thermal conductivity?

In this paper, for the first time, we fully address these questions by high-throughput quantum mechanical calculations including up to fourth-order anharmonicity and four-phonon scattering, considering Li_xCoO_2 ($x = 1, 0.67, 0.5, 0.33$) and Li_xNbO_2 ($x = 1, 0.5$) as prototype examples. We predict that the thermal conductivities are significantly lower than hitherto believed. The origins of the ultra-low thermal conductivities are as follows:

(1) The fourth-order anharmonicity in these materials is strong and the impact of four-phonon scattering is significant. As a result, the intrinsic thermal conductivity is much smaller than has been predicted without inclusion of these phenomena. The intrinsic in-plane and through-plane thermal conductivities are 9.7 and 1.4 $Wm^{-1}K^{-1}$ for $LiCoO_2$, in contrast to previously predicted [29,30,32,33] 19.8–53.6 $Wm^{-1}K^{-1}$ and 2.2–8.4 $Wm^{-1}K^{-1}$, respectively. In comparison to $LiCoO_2$, weaker anharmonicity is present in $LiNbO_2$ because Nb has fewer lone electrons than Co.
(2) Charging (delithiation) is another significant effect that reduces κ. It strongly softens the lattice, reduces phonon velocities (especially in the through-plane direction), increases the anisotropic ratio, and increases anharmonicity as well as the three- and four-phonon scattering rates in all Li_xTMO_2 studied in this work. The calculated κ matches available experimental data only when four-phonon scattering is included, supporting the significance of high-order anharmonicities as well as the validity of the present calculations.
(3) Grain size is another factor that is responsible for the ultra-low κ of $LiTMO_2$ polycrystals. Although four-phonon scattering reduces the phonon mean free paths and thus weakens the grain-boundary effect, κ of $LiCoO_2$ and $LiNbO_2$ can still be reduced by 26% and 60%, respectively, when grain size is reduced down to 10 nm.
(4) Internal strains significantly tune the thermal conductivity by changing the phonon scattering phase space. 2% compressive strain increases the thermal conductivity by 30–80% (depending on the direction), while 2% tensile strain diminishes the thermal conductivity. Also, we find that the vibration frequency of Li is exceptionally sensitive to strain and may be used to determine the strain in experiments.
(5) The impact of Li diffusion on the thermal transport is negligible since the hopping rate is much smaller than the phonon scattering rates. Other possible factors such as electronic thermal conductivity and porosity are also discussed. These results elucidate long-standing questions regarding thermal transport in Li_xTMO_2 and provide valuable insights that can guide the design of next-generation batteries and electronics.

2. Methods

A detailed description of the methods and formalism is given in the Supplemental Information. Here, we briefly introduce the methodology that we used. The thermal conductivity of single crystals is calculated using exact solutions of the Boltzmann transport equation in the phonon-relaxation-time approximation, including three- and four-phonon scattering. Density functional theory calculations are carried out to produce the 2nd-, 3rd-, and 4th-order interatomic force constants. Fermi's golden rule is used to evaluate the three- and four-phonon scattering rates. After we obtained the intrinsic anisotropic thermal conductivities of the crystals, we use an orientation average to evaluate the thermal conductivity of polycrystals. To account for the impact of delithiation, we remove varying amounts of Li atoms from the unit cells and recalculate all the force constants and phonon scattering rates. We then add an extra scattering term, accounting for phonon-Li disorder scattering, in addition to the intrinsic phonon-phonon scattering, to calculate the thermal conductivity. When the grain size is comparable to or even smaller than the phonon mean free path, the grain boundary could confine the phonons from propagating, and therefore reduce the phonons' contribution to the thermal conductivity.

3. Results and discussion

3.1. Vibrational and thermal properties and the impact of delithiation

We start by discussing the calculated vibrational properties of $LiCoO_2$ in the atomic structure shown in Fig. 1 **a**. Lithium atoms are intercalated in-between CoO_2 layers. The through-plane arrangement of these layers is the ABC structure, or O3 structure, based on the classification by Refs. [34]. The phonon dispersion and projected density of states (pDOS) are shown in Fig. 1 **b** and **g**. It is found that the Co, Li, and O species have distinct ranges of vibrational frequencies, i.e., they dominate the low-, mid-, and high-frequency ranges, respectively. Co has the highest atomic mass and therefore vibrates most slowly. Li atoms, although being the lightest, are bonded loosely in the lattice, and therefore vibrate more slowly than O atoms, which bond strongly in the lattice with Co atoms and vibrate most rapidly.

To examine the effects of gradual charging (removing Li from Li_xCoO_2), we calculated the phonon dispersions and pDOS of Li_xCoO_2 for $x = 0.67$, 0.5, and 0.33. As shown in Supplementary Figs. S1 and S2, the Li_xTMO_2 crystalline structures structures at certain x values are obtained by removing Li atoms periodically and keeping the smallest possible unit cell after Li removal. These structures are all obtained from the Materials Project [35]. For example, in $Li_{0.67}CoO_2$, the remaining Li atoms form a graphene-like structure with the center Li in each hexagonal ring removed. In $Li_{0.33}CoO_2$, the Li removal is reversed, i.e., the center Li in each hexagonal ring is kept while all Li atoms on hexagonal rings are removed. In $Li_{0.5}CoO_2$, Li is removed from every other row in each layer, leaving half the number of Li atoms remaining in the lattice. $LiNbO_2$ has a similar layered intercalation structure with $LiCoO_2$ but with a different

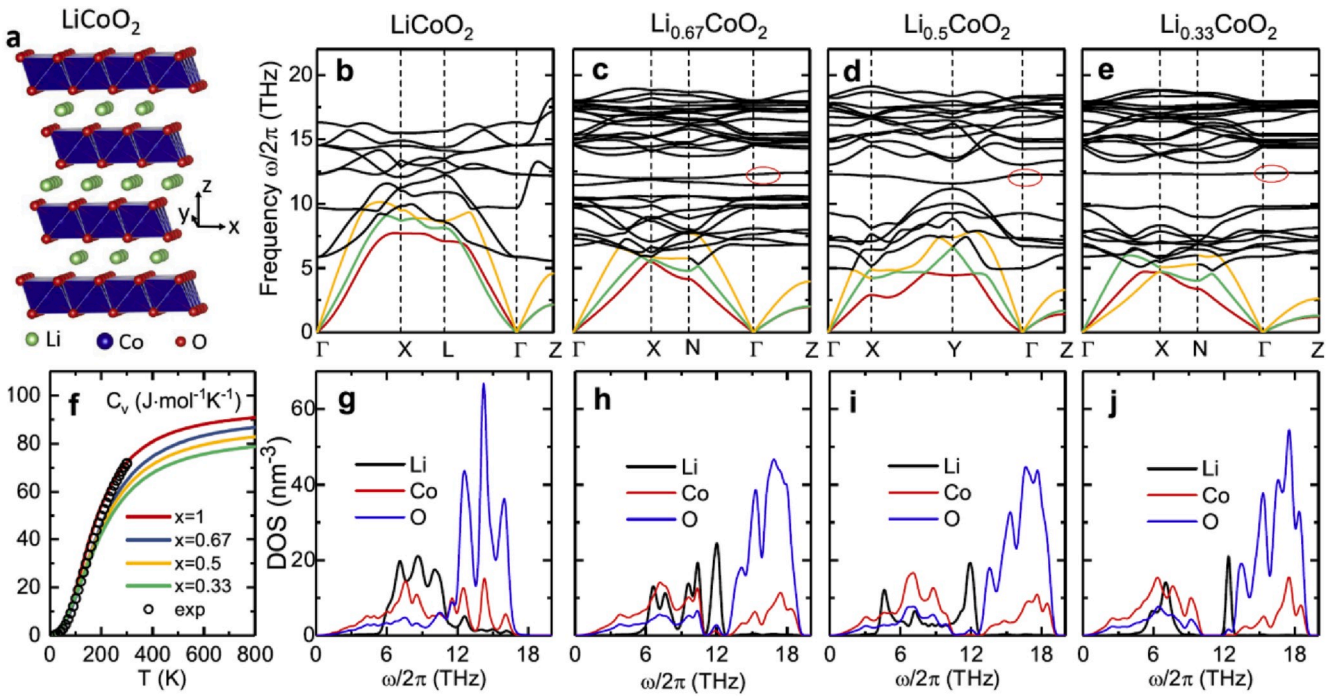

Fig. 1. Harmonic vibrational properties of Li_xCoO_2 (x = 1, 0.67, 0.5, 0.33). a, Crystal structure of $LiCoO_2$. **b-e**, Phonon dispersion relations of Li_xCoO_2. The colored curves highlight acoustic branches. The red circles in **c-e** highlight the flat band dominated by Li vibrations. **f**, Heat capacities of Li_xCoO_2 as functions of temperature, compared to experimental data [36]. **g-j**, Atomic-site-projected phonon densities of states. (For interpretation of the references to color in this figure legend, the reader is referred to the Web version of this article.)

stacking order of ABAB. The Li atoms in all layers are overlapped in the top view. The creation of crystalline delithiated Li_xNbO_2 structures is similar to that of $LixCoO_2$. The phonon dispersion and harmonicity are calculated based on the crystalline Li_xTMO_2 structures, while the lithium disorder is taken into account by including an extra Li disorder phonon-scattering term in the thermal conductivity calculations. The results, shown in Fig. 1 **c-e,** respectively, reveal an interesting phenomenon: the lower phonon branches of $LiCoO_2$ gradually move to even lower energies (they soften) while the upper branches move to even higher energies (they stiffen), generating a gap between them. We further track these changes in Fig. 1 **h-j**, where we compare the phonon pDOS of the Li, Co, and O species and relate the changes to the atomic structures (more comparisons are included in Supplementary Figs. S3–S5). We find that the softening of lower branches is effected by Co and Li while the stiffening of upper branches is dominated by Co and O. When the Li concentration is sufficiently high, Li atoms act as linkages between adjacent CoO_2 layers by attracting O^{2-} ions. We conclude that Li loss leads to a weakening of the interlayer bonding strength and hence softening of the lower phonon branches, which describe the in-phase vibrations of the lattice. These features also explain the softening of the bulk modulus during delithiation observed in experiments [24]. In contrast, interlayer softening is accompanied by intralayer stiffening, i.e., the binding between Co and O becomes stronger. This strengthening arises because the valence of Co increases from +3 to +3+(1-x) after delithiation, which strengthens the Coulombic interaction between Co^{3+1-x} and O^{2-} ions. As a result, the upper phonon branches move to even higher energies because they are dominated by out-of-phase vibrations between the Co^{3+1-x} and O^{2-} ions. In addition, we note that, after delithiation, a flat band at around 12 THz lies between the lower and upper branches. The eigenvector shows that this mode is the through-plane vibration of Li atoms, as can be seen in the pDOS of Li in Fig. 1 **h-j**. This feature indicates that Li is loosely bonded in the lattice and can rattle between the layers. All these characteristics found in the vibrational properties provide physical insights into the thermal transport as will be discussed later in this paper.

The impact of delithiation on phonon velocities is also significant. Generally, the group velocities of most phonon modes are significantly reduced as the lattice becomes softer during delithiation (Supplementary Figs. S6–S9). Especially, the velocities of the phonons associated with through-plane vibrations, regardless of transport direction, are softened. For example, the through-plane long-wavelength longitudinal-acoustic ($v_{\perp,LA}$) and transverse-acoustic ($v_{\perp,TA}$) phonon velocities decrease from 5.6 and 3.0 km/s to 3.7 and 1.9 km/s, respectively, when x decreases from 1 to 0.33 in Li_xCoO_2. Most in-plane phonon velocities are reduced as well, except for the long-wavelength (in-phase) $v_{\perp,LA}$ and $v_{\perp,TA}$, which increase with delithiation due to the in-plane stiffening discussed above. This result is analogous to the phonon-focusing effect [37], by which compression of a lattice in one direction reduces the phonon velocity in the perpendicular direction since phonon wavevectors gain a larger projection along the compressed direction.

The heat capacity C_v of Li_xCoO_2, which is also determined by the vibrational spectra, is also strongly affected by delithiation. As shown in Fig. 1 **f**, C_v increases with temperature and saturates above 800 K, agreeing well with available experimental data [36]. Upon delithiation, the room-temperature (RT) C_v decreases almost linearly with decreasing Li concentration at a rate of 0.2 J mol^{-1} K^{-1} per 1 at%Li (Supplementary Fig. S10). Full delithiation can lead to 28% loss of heat capacity, which indicates a faster temperature rise at low Li concentrations, given the same amount of Joule heat.

Although so far we have discussed the vibrational properties of Li_xCoO_2, the characteristics and the impact of delithiation are equally applicable to Li_xNbO_2 (Supplementary Figs. S11–S15), possibly indicating general trends in layered Li_xTMO_2.

3.2. Third and fourth-order anharmonicities and phonon scattering rates

Lattice anharmonicity determines the thermal resistance of a system. Previously, most studies were based on the lowest order anharmonicity, i.e., third-order anharmonicity and three-phonon scattering [38–40]. Beginning in 2016, Feng et al. [26–28], computed fourth-order

anharmonicity and four-phonon scattering and found that their effect on thermal transport can be significant. However, the capability of those four-phonon studies was limited to simple systems with two basis atoms per unit cell. The 4–14 basis atoms per unit cell in the Li_xTMO_2 systems make the four-phonon scattering calculations extremely demanding. Here, we calculate the third-order anharmonicity and three-phonon scattering for all the materials, and then take $LiCoO_2$, $Li_{0.33}CoO_2$, $LiNbO_2$ and $Li_{0.5}NbO_2$ to explore the significance of fourth-order anharmonicity and four-phonon scattering by using high-throughput calculations.

The comparison of the anharmonicities between two materials is done by comparing their largest values of the anharmonic force constants (AFCs) and their counts (when AFCs values are close). See Supplementary Section 2 for details of the counting mechanism of AFCs and the rationale of qualitative or quantitative interpretation. Compared to the previous method of qualitatively comparing certain anharmonic vibrational potential wells [41], the present method is more accurate as it quantifies all significant anharmonic potential wells in the systems. Fig. 2 shows the third- and fourth-order AFCs for **a**, $LiCoO_2$ and $LiNbO_2$, **b**, $LiCoO_2$ and $Li_{0.33}CoO_2$, and **c**, $LiNbO_2$ and $Li_{0.5}NbO_2$. Several representative relations between anharmonicities and coordinates, TM species, as well as Li concentrations are revealed:

(1) Most of the largest AFCs are associated with the through-plane vibrations.
(2) Most of the significant AFCs are associated with TM or O atoms, rather than Li atoms.
(3) $LiCoO_2$ is more anharmonic than $LiNbO_2$ in the third order and is much more so in the fourth order, which may originate from the fact that Co ($4s^23\ d^7$) has more lone electrons than Nb ($5s^14\ d^4$) after binding with O. These lone electrons serve as a buffer that softens the vibrations [42].
(4) $Li_{0.33}CoO_2$ and $Li_{0.5}NbO_2$ are much more anharmonic than $LiCoO_2$ and $LiNbO_2$ in both third and fourth orders, demonstrating the increase of anharmonicity with delithiation.

To sum up, the above comparisons reveal that the interaction between TM and O becomes more anharmonic with the loss of Li atoms in $LiCoO_2$, $LiNbO_2$, and possibly other layered Li_xTMO_2, which provides valuable insight for understanding the thermal transport.

With third and fourth order AFCs, the three and four-phonon scattering rates of Li_xCoO_2 and Li_xNbO_2 are calculated. Distinctly, as shown in Fig. 3 **a**-**d**, we find that four-phonon rates are substantial for most of the materials of interest here, providing a critical revisit of prevailing knowledge [30]. Among the four materials, $LiNbO_2$ is the least anharmonic and has the lowest three- and four-phonon scattering rates, consistent with the conclusions drawn from the analyses of AFCs. Compared to the well-known three-phonon scattering, four-phonon scattering has never been explored in complex crystals yet and is of particular interest. To gain deeper insight, we decompose the overall four-phonon scattering into the *splitting* ($\lambda \rightarrow \lambda' + \lambda'' + \lambda''' + \boldsymbol{R}$), *redistribution* ($\lambda + \lambda' \rightarrow \lambda'' + \lambda''' + \boldsymbol{R}$), and *recombination* ($\lambda + \lambda' + \lambda'' \rightarrow \lambda''' + \boldsymbol{R}$) categories and distinguish the Normal ($\boldsymbol{R} = 0$) from Umklapp processes ($\boldsymbol{R} \neq 0$), where $\lambda = (\boldsymbol{q}, j)$, a shorthand for a phonon mode with wavevector $\boldsymbol{q}$ and dispersion branch j. $\boldsymbol{R}$ can be any reciprocal lattice vector. The decomposed four-phonon scattering rates in $LiCoO_2$ are shown in Fig. 3 **e** (similar plots for $Li_{0.33}CoO_2$, $LiNbO_2$, and $Li_{0.5}NbO_2$ can be found in Supplementary Fig. S16). Clearly, four-phonon scattering is dominated by the Umklapp *redistribution* processes in all four materials. Taking a further step, we find that this is due to the large number of available combinations of $(\lambda', \lambda'', \lambda''')$ that satisfy both energy and momentum conservation rules for the $\lambda + \lambda' \rightarrow \lambda'' + \lambda''' + R$ process, as shown in Fig. 3 **f**. These processes are most intensive in the mid-frequency range. We also note another significant phenomenon, i.e., the four-phonon scattering rates of upper optical branches are not as high as expected in the literature on simple crystals [26,27], which is important for understanding the optical properties of complex materials.

3.3. Lattice thermal conductivity

The lattice thermal conductivity of $LiCoO_2$ single crystal calculated by first principles is shown in Fig. 4 **a**. Throughout the paper, the thermal conductivity predicted without and with four-phonon scattering are represented by κ_3 and κ_{3+4}, or $\kappa(3)$ and $\kappa(3+4)$, respectively. Four-phonon scattering reduces the room-temperature intrinsic in-plane κ ($\kappa_\parallel$) from 26.3 to 9.7 $Wm^{-1}K^{-1}$, and through-plane κ ($\kappa_\perp$) from 3.8 to 1.4 $Wm^{-1}K^{-1}$, providing significant revision to the prevailing knowledge [29,30,32,33] which predicted 19.8–53.6 $Wm^{-1}K^{-1}$ and 2.2–8.4 $Wm^{-1}K^{-1}$ for $\kappa_\parallel$ and $\kappa_\perp$, respectively. The κ reduction due to fourth-order anharmonicity is as large as 60% for both directions at room temperature, and increases to 83% as the temperature climbs to 900 K.

The predicted κ of Li_xCoO_2 after delithiation to x(Li) = 0.33 is shown in Fig. 4 **b**. The $\kappa_{\parallel,3+4}$ and $\kappa_{\perp,3+4}$ are 6.5 and 0.41 $Wm^{-1}K^{-1}$, respectively, which are 33% and 70% smaller than that of $LiCoO_2$. Thus, we conclude that the loss of Li significantly affects the thermal transport, especially in the through-plane direction. In $Li_{0.33}CoO_2$, we find that the room-temperature κ reduction due to fourth-order anharmonicity is 36%, which is smaller than that in $LiCoO_2$. This is because the importance of fourth-order anharmonicity is overwhelmed by the loss of Li in reducing

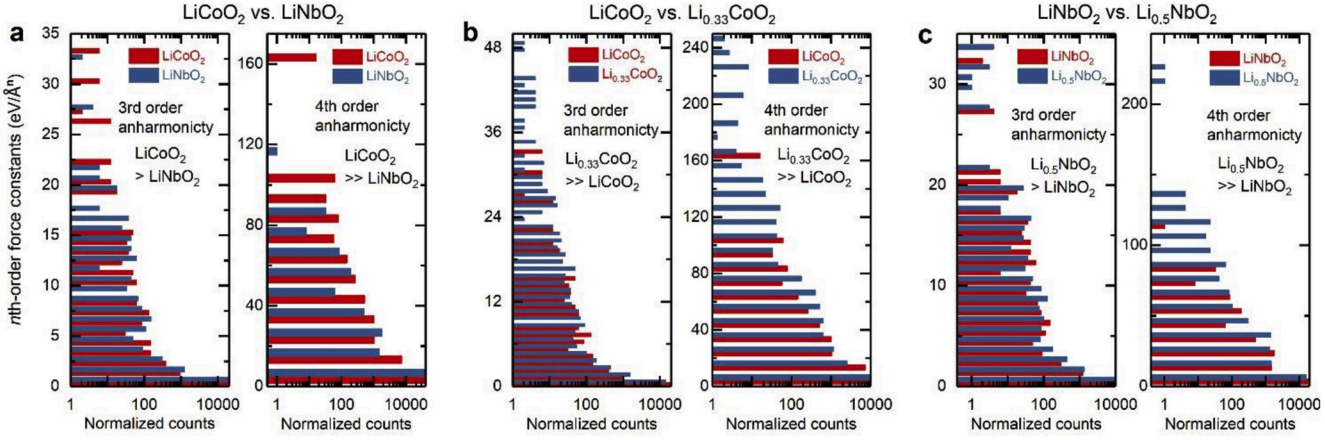

Fig. 2. Third and fourth-order anharmonicities of Li_xCoO_2 and Li_xNbO_2. **a**, Comparison between $LiCoO_2$ and $LiNbO_2$. **b**, Comparison between $LiCoO_2$ and $Li_{0.33}CoO_2$. **c**, Comparison between $LiNbO_2$ and $Li_{0.5}NbO_2$. The subfigures count the number of force-constant values in certain ranges. The counts of each material are normalized by the number of TMO_2 in a unit cell.

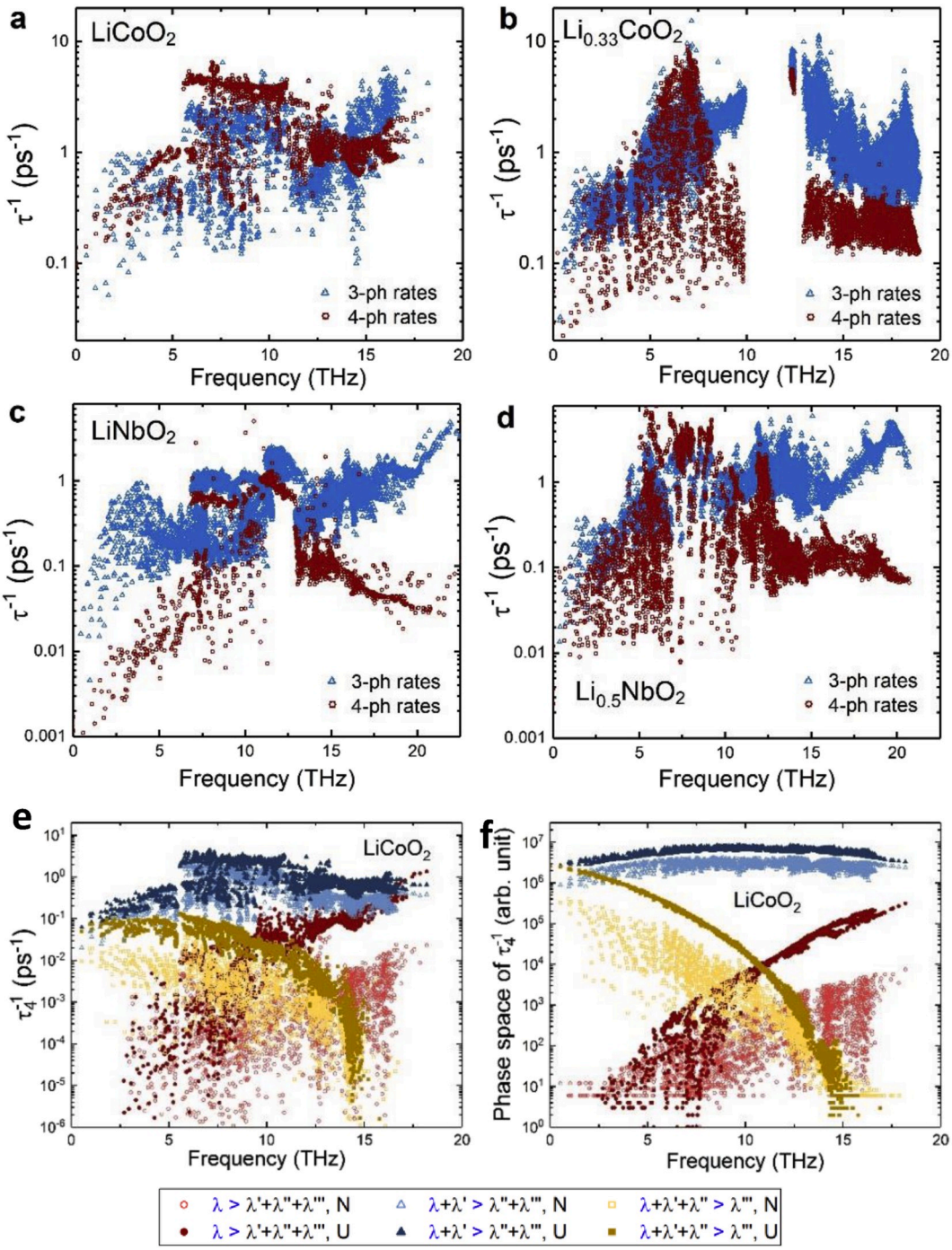

Fig. 3. Full-Brillouin zone anharmonic three- and four-phonon scattering rates in Li_xCoO_2 and Li_xNbO_2 at room temperature. a-d, Three and four-phonon scattering rates in $LiCoO_2$, $Li_{0.33}CoO_2$, $LiNbO_2$, and $Li_{0.5}NbO_2$, respectively. **e**, Decomposed four-phonon scattering rates in $LiCoO_2$. **f.** Decomposed numbers of possible four-phonon scattering events in $LiCoO_2$. In **e** and **f**, the normal processes and Umklapp processes are represented by open and solid symbols, respectively. The splitting ($\lambda \rightarrow \lambda' + \lambda'' + \lambda'''$), redistribution ($\lambda + \lambda' \rightarrow \lambda'' + \lambda'''$), and recombination ($\lambda + \lambda' + \lambda'' \rightarrow \lambda'''$) processes are represented by red, blue and yellow colors, respectively. (For interpretation of the references to color in this figure legend, the reader is referred to the Web version of this article.)

κ.

Compared to Li_xCoO_2, Li_xNbO_2 has much larger thermal conductivity as shown in Fig. 4 **c-d**. $\kappa_{\parallel}$ and $\kappa_{\perp}$ are 31.5 and 5 $Wm^{-1}K^{-1}$ for $LiNbO_2$, and 10.6 and 1.1 $Wm^{-1}K^{-1}$ for $Li_{0.5}NbO_2$ single crystals, respectively. The effect of four-phonon scattering is smaller compared to Li_xCoO_2 but still non-negligible. However, the κ reduction due to delithiation is substantially stronger: delithiation to x(Li) = 0.5 leads to a reduction of 66% and 78% for $\kappa_{\parallel}$ and $\kappa_{\perp}$, respectively. Such significant reduction may pose potential challenge for Li_xNbO_2 batteries [7], but gives promise for Li_xNbO_2 thermoelectrics [43]. We also note that the κ anisotropic ratio for Li_xCoO_2, Li_xNbO_2, and possibly other layered Li_xTMO_2 materials is large and increases with delithiation, which may provide promise for the further new-directional thermal management.

To compare with available experimental data [24,43] and validate the present calculation of four-phonon scattering, we convert the calculated anisotropic thermal conductivity ($\kappa_{\parallel,\perp}$) of single crystals to the orientation-average thermal conductivity (κ_a) of polycrystals (see Supplementary Section 3 for details). Clearly, κ_a strongly depends on the

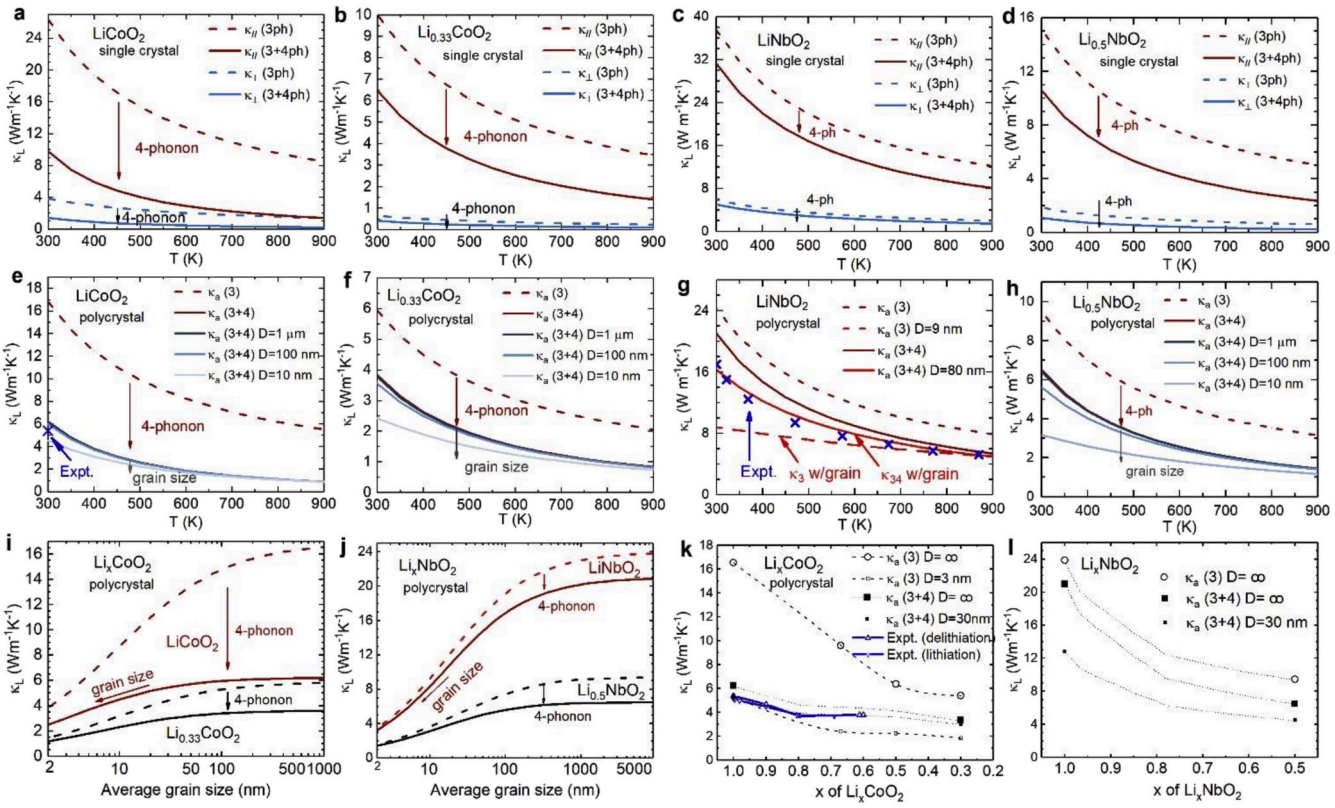

Fig. 4. Lattice thermal conductivities κ_L of Li_xCoO_2 and Li_xNbO_2 predicted by first principles. In all the panels, dashed and solid curves represent the predictions with and without four-phonon scattering, respectively. **a-d**, In-plane (||) and through-plane (⊥) thermal conductivities of $LiCoO_2$, $Li_{0.33}CoO_2$, $LiNbO_2$, and $Li_{0.5}NbO_2$ single crystals as functions of temperature. **e-h**, Orientation-averaged thermal conductivities (κ_a) of $LiCoO_2$, $Li_{0.33}CoO_2$, $LiNbO_2$, and $Li_{0.5}NbO_2$ polycrystals as functions of temperature. The predictions with various grain sizes (D) are also included. **i,j**, Room-temperature polycrystalline thermal conductivities, κ_a(300K), as functions of grain diameter (D). **k,l**, κ_a(300K) as functions of Li concentration x. In **k** and **l**, the dotted curves connecting the four-phonon predictions are drawn to guide eyes. Experimental data of Li_xCoO_2 and $LiNbO_2$ are taken from Ref. [24] and Ref. [43], respectively.

temperature, grain size D, and lithium concentration x, as shown in Fig. 4 **e-h**, **i-j**, and **k-l**, respectively. Since the calculated $\kappa_a(3)$ and $\kappa_a(3+4)$ depend on D, which was not determined in experimental works [24,43], it is not reasonable to validate $\kappa_a(3)$ or $\kappa_a(3+4)$ by doing a single κ value comparison since D is an adjustable fitting parameter, which can be adjusted arbitrarily to match experimental κ_{exp}. However, we can validate the necessity and accuracy of four-phonon scattering calculations by comparing the T dependency since $\kappa_a(3+4)$ decreases faster than $\kappa_a(3)$ with T, especially when defects or grain boundaries are presented [26–28]. For example, as shown in Fig. 4 **g** by the red dashed line, the experimental data cannot be fitted well without inclusion of four-phonon scattering. Although a D value can be chosen for $\kappa_a(3)$ to match κ_{exp} at a single temperature (900 K, for example), this D value results in disagreement at all the other temperatures. In contrast, $\kappa_a(3+4)$ can match the experimental data throughout the whole temperature range with an appropriate D value. Similarly, the validation can also be done by comparing the lithium concentration (x) dependency, as shown in Fig. 4 **k**. That is, although a D value can be chosen for $\kappa_a(3)$ to match κ_{exp} at a single x ($x = 0$, for example), this D value results in disagreement at all the other x values, while $\kappa_a(3+4)$ can match with experimental data throughout the whole x range with an appropriate D value. In addition, in comparison to the $D = 3$ nm fitted by using $\kappa_a(3)$, the fitted D by using $\kappa_a(3+4)$ is about 30 nm, which agrees better with the 20–50 nm shown in the high-resolution transmission-electron-microscopy images of Ref. [24]. To summarize, by validating the predicted $\kappa_a(3+4)$ with available experimental data [24,43] through different perspectives for different materials with broad temperature and lithium concentration ranges, it is safe to conclude the significance of four-phonon scattering in Li_xCoO_2 and Li_xNbO_2 and the accuracy of the present work.

To gain more insight into the thermal transport, we investigate the spectral thermal conductivity contributions in these materials. It is found that $\kappa_{\parallel}$ of $LiCoO_2$ and $Li_{0.33}CoO_2$ are contributed by the phonons with frequencies 0–10 THz and 0–5 THz, respectively. The $\kappa_{\perp}$ comes from 0-5 THz and 0–3 THz, respectively (Supplementary Fig. S17). These frequency ranges have little overlap with the Li pDOS, indicating that the vibrations of Li ions are localized and do not contribute to the thermal transport. The results also indicate that, with delithiation, the lower-branch acoustic phonons are more dominant in thermal transport. This dominance of the lower-branch acoustic phonons occurs because the higher phonon branches (dominated by strong interactions between Co^{4-x} and O^{2-}) become more anharmonic as discussed in the preceding text. Similar conclusions are also applied to Li_xNbO_2 (Supplementary Fig. S18). The phonon relaxation times of the lower branches are 1–2 orders of magnitude longer than the upper branches (Supplementary Figs. S19–S26).

3.4. Significant strain effect

During the charging/discharging process, large strains can be accumulated [5,44,45], with Li_xCoO_2 being able to sustain as large as 30% through-plane strain [46]. The strain impact on the mechanical, electrical, and ionic transport properties have been extensively studied [46–49], while the impact on thermal transport is still unclear. Taking delithiated Li_xCoO_2 (x = 0.33) for example, we investigated the strain effect on the harmonic and third-order anharmonic properties under 2% (tensile), −2% (compressive), −5% (compressive), and −10% (compressive) strains along the z direction. We find that, remarkably,

apart from the slight softening or stiffening effect due to the tensile or compressive strains, there is an exceptional variation in the vibrations of Li atoms under strain (Supplementary Figs. S27–S31). As shown in Fig. 5 **a**, the Li vibrations shift significantly with the applied strain, with approximately a linear rate of 0.4 and 0.3 THz per 1% strain, i.e., 11 and 8 cm^{-1} per GPa, for the two peak frequencies in the pDOS. The shifting rates are more than 1 order of magnitude larger than those of other modes. The main reason is that the bonding of Li with the other atoms is very weak and highly dependent on the distance to the adjacent TMO_2 layers. A slight change in the interlayer spacing due to strain can therefore have a large effect on the vibrational frequency of Li. Inspired by the temperature measurement via temperature-dependent frequency shifts [50], we propose that the strong strain-dependent Li partial DOS provides a potential tool to measure the strain of Li_xCoO_2 in experiments. For example, by using either optical methods such as Raman and infrared spectroscopy or electron methods such as electron energy loss spectroscopy (EELS), the lithium phonon energy can be measured and then the average strain in the sample can be obtained. If an electron method is used, the measurement may also have high spatial resolution so that variations in the local strain of the material can be detected.

In addition to the remarkable change in harmonic vibrations, we find that strain has surprising impact on the thermal conductivity as well. As shown in Fig. 5 **b**, 2% tensile strain can nearly diminish the three-phonon κ_3 of $Li_{0.33}CoO_2$. 2% compressive strain can increase κ_3 by 30% and 80% for the $\kappa_{\parallel}$ and $\kappa_{\perp}$, respectively. The origin of such surprisingly large impact of strain is elucidated by comparing the three factors that determine κ: phonon velocities, anharmonicities, and scattering phase space. It turns out that the velocities and anharmonicities do not vary significantly with strain (Supplementary Figs. S32 and S33), while the scattering phase space depends strongly on strain due to the change in Li pDOS (Supplementary Fig. S34). With compressive strains, the phonon dispersion tends to spread out, and the energy spacing between different phonon branches enlarges. As a result, the phonon-phonon scattering probability decreases since the energy conservation rule is not as easily satisfied compared to more crowded branches. Therefore, the phonon scattering rate is reduced and the phonon relaxation time is increased, leading to a sharp increase of thermal conductivity. With tensile strains, the scenario is reversed. Note that these κ_3 values are not the exact thermal conductivities of materials since four-phonon scattering or *diffuson* contribution [51] is not included in the calculation of κ_3. Nevertheless, studying κ_3 is enough to reveal the general impact of strain on anharmonicity.

The calculated phonon scattering rates and intrinsic κ in the preceding text can enable the estimation of the impact of other effects, including ionic diffusion, electrical conductivity, and porosity, on the thermal transport. These effects are of great interest for both fundamental physics and practical application in batteries and memristors. The thermal conductivity derived from vibrational properties assumes that the atoms vibrate around fixed positions, i.e., their equilibrium positions, and do not migrate around. It has, therefore, been a persistent question whether the diffusion of atoms makes a difference to the thermal conductivity of the materials with high ionic mobility [52]. With detailed analysis shown in Supplementary Section 18, 19 and 20, we conclude that the impact of Li diffusion and electrical conductivity on the thermal properties of Li_xCoO_2 is negligible, and the impact of porosity is large in experimental cathodes since they are usually porous. This impact can be readily predicted by using the effective medium approximation.

The analysis in this work is mainly based on layered Li_xTMO_2; however, we expect that most conclusions of this study can also be applied to other Li-based TMOs such as $LiMn_2O_4$ (spinel structure) and $LiFePO_4$ (olivine structure). For example, most of these Li-intercalation materials are also likely to have strong high-order lattice anharmonicity and four-phonon scattering (due to the soft bonding of Li and the anharmonic Coulombic interaction between TM and O atoms), strong impact of delithiation, strong effect of grain boundaries, and negligible impact of Li fluidity. Nevertheless, the impact of strain in $LiMn_2O_4$ and $LiFePO_4$ is not necessarily as large as that in layered Li_xTMO_2 in which the through-layer strain can easily change the Li bonding environment.

4. Conclusions

To conclude, by considering up to the fourth order quantum lattice anharmonicity and four-phonon scattering, we have resolved several long-standing, fundamental, yet practically important questions regarding the vibrational and thermal properties of $LiCoO_2$, $LiNbO_2$ and possibly other layered Li_xTMO_2 that are crucial for battery and memristors applications. In particular, we showed that (1) the intrinsic thermal conductivities of $LiCoO_2$ and $LiNbO_2$ are 2–6 times lower than those predicted by prior theories due to strong four-phonon scattering; (2) although Li vibrations do not contribute to the thermal conductivity, the delithiation process can result in significant decrease of thermal conductivity of $LiTMO_2$ due to the softening of interlayer bonding as well as the increase of phonon-vacancy scattering; (3) the thermal conductivity of $LiTMO_2$ polycrystals can be tuned by several times through tuning of the grain size; (4) the internal compressive or tensile strain induced during charge/discharge cycles can enhance or reduce the $LiTMO_2$ thermal conductivity multiple times. These findings are expected to generate broad impact not only on the fundamental thermal physics of complex oxides but also on the development of next-generation batteries and memristors.

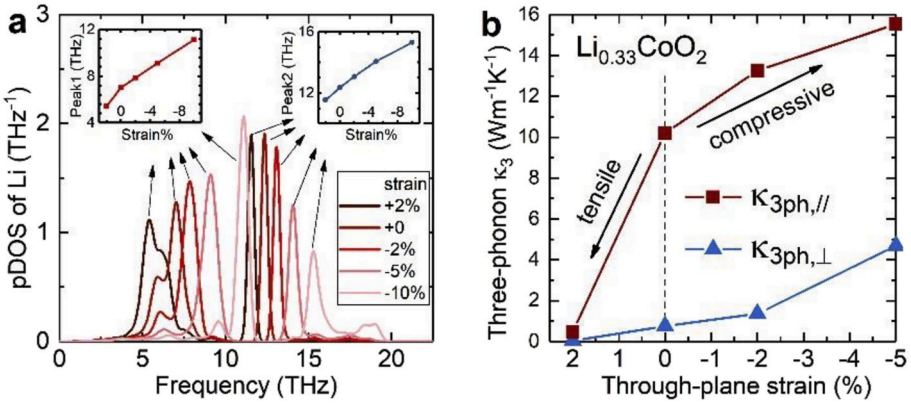

Fig. 5. Exceptional strain impact on thermal properties of Li_xCoO_2. a, Projected phonon DOS on Li in $Li_{0.33}CoO_2$ with +2%, 0, −2%, −5%, −10% through-plane strains. The insets show the shifts of the two peak frequencies as functions of strain. **b**, Room-temperature in-plane and through-plane three-phonon thermal conductivity of $Li_{0.33}CoO_2$ under various through-plane strains.

Author contributions

T.F. and S.T.P. conceived the project. T.F. conducted the simulations and wrote the manuscript. A.O. contributed to simulations and discussions. All authors contributed to the manuscript.

Additional information

Supplementary information including computational methodology is available in the online version of the paper. Correspondence and requests for materials should be addressed to T.F. and S.T.P.

Declaration of competing interest

The authors declare no competing financial interests.

CRediT authorship contribution statement

Tianli Feng: Conceptualization, Data curation, Formal analysis, Investigation, Methodology, Visualization, Writing - original draft. **Andrew O'Hara:** Investigation, Writing - review & editing. **Sokrates T. Pantelides:** Funding acquisition, Resources, Supervision, Writing - review & editing.

Acknowledgements

This work is supported in part by the U.S. Department of Energy (DOE), Office of Science, Office of Basic Energy Sciences (BES), Materials Sciences and Engineering Division under Award DE-FG0209ER46554 and by the Vanderbilt McMinn Endowment. T.F. also acknowledges support from the DOE Office of Energy Efficiency & Renewable Energy (EERE), Building Technologies Office. Computations were performed at the National Energy Research Scientific Computing Center (NERSC), a Department of Energy, Office of Science, User Facility funded through Contract No. DE-AC02-05CH11231. Computations also used the Extreme Science and Engineering Discovery Environment (XSEDE).

Appendix A. Supplementary data

Supplementary data to this article can be found online at https://doi.org/10.1016/j.nanoen.2020.104916.

References

[1] K. Mizushima, P.C. Jones, P.J. Wiseman, J.B. Goodenough, LixCoO2 (0<x≤1): a new cathode material for batteries of high energy density, Solid State Ionics 3–4 (1981) 171–174.
[2] D. Castelvecchi, E. Stoye, Chemistry Nobel honours world-changing batteries, Nature 574 (2019), 308–308.
[3] J.B. Goodenough, Y. Kim, Challenges for rechargeable Li batteries, Chem. Mater. 22 (2010) 587–603.
[4] C. Choi, et al., Achieving high energy density and high power density with pseudocapacitive materials, Nat. Rev. Mater. (2019), https://doi.org/10.1038/s41578-019-0142-z.
[5] J.N. Zhang, et al., Trace doping of multiple elements enables stable battery cycling of LiCoO2 at 4.6 V, Nat. Energy 4 (2019) 594–603.
[6] Q. Liu, et al., Approaching the capacity limit of lithium cobalt oxide in lithium ion batteries via lanthanum and aluminium doping, Nat. Energy 3 (2018) 936–943.
[7] W. Li, et al., The electrochemical synthesis of LiNbO2in molten salts and its application for lithium ion batteries with high rate capability, Electrochim. Acta 189 (2016) 231–236.
[8] V.H. Mai, et al., Memristive and neuromorphic behavior in a LixCoO2 nanobattery, Sci. Rep. 5 (2015) 7761.
[9] Q. Hu, et al., Lithium ion trapping mechanism of SiO2 in LiCoO2 based memristors, Sci. Rep. 9 (2019) 5081.
[10] J.D. Greenlee, et al., Radiation effects on LiNbO2 memristors for neuromorphic computing applications, IEEE Trans. Nucl. Sci. 60 (2013) 4555–4562.
[11] J.D. Greenlee, et al., In-situ oxygen x-ray absorption spectroscopy investigation of the resistance modulation mechanism in LiNbO2memristors, Appl. Phys. Lett. 100 (2012), 0–4.
[12] J.J. Yang, D.B. Strukov, D.R. Stewart, Memristive devices for computing, Nat. Nanotechnol. 8 (2013) 13–24.
[13] D.B. Strukov, G.S. Snider, D.R. Stewart, R.S. Williams, The missing memristor found, Nature 453 (2008) 80–83.
[14] M.A. Zidan, J.P. Strachan, W.D. Lu, The future of electronics based on memristive systems, Nat. Electron. 1 (2018) 22–29.
[15] P. Canepa, et al., Odyssey of multivalent cathode materials: open questions and future challenges, Chem. Rev (2017), https://doi.org/10.1021/acs.chemrev.6b00614 acs.chemrev.6b00614.
[16] P. Albertus, S. Babinec, S. Litzelman, A. Newman, Status and challenges in enabling the lithium metal electrode for high-energy and low-cost rechargeable batteries, Nat. Energy 3 (2018) 16–21.
[17] Y. Sun, N. Liu, Y. Cui, Promises and challenges of nanomaterials for lithium-based rechargeable batteries, Nat. Energy 1 (2016).
[18] R. Schmuch, R. Wagner, G. Hörpel, T. Placke, M. Winter, Performance and cost of materials for lithium-based rechargeable automotive batteries, Nat. Energy 3 (2018) 267–278.
[19] K. Liu, Y. Liu, D. Lin, A. Pei, Y. Cui, Materials for lithium-ion battery safety, Sci. Adv. 4 (2018).
[20] Y. Liu, Y. Zhu, Y. Cui, Challenges and opportunities towards fast-charging battery materials, Nat. Energy 4 (2019) 540–550.
[21] J. Deng, C. Bae, J. Marcicki, A. Masias, T. Miller, Safety modelling and testing of lithium-ion batteries in electrified vehicles, Nat. Energy 3 (2018) 261–266.
[22] M. Hao, J. Li, S. Park, S. Moura, C. Dames, Efficient thermal management of Li-ion batteries with a passive interfacial thermal regulator based on a shape memory alloy, Nat. Energy 3 (2018) 899–906.
[23] M.-T.F. Rodrigues, et al., A materials perspective on Li-ion batteries at extreme temperatures, Nat. Energy 2 (2017) 1–14.
[24] J. Cho, et al., Electrochemically tunable thermal conductivity of lithium cobalt oxide, Nat. Commun. 5 (2014) 1–6.
[25] Y. Zhu, et al., Fast lithium growth and short circuit induced by localized-temperature hotspots in lithium batteries, Nat. Commun. 10 (2019) 1–7.
[26] T. Feng, X. Ruan, Quantum mechanical prediction of four-phonon scattering rates and reduced thermal conductivity of solids, Phys. Rev. B 93 (2016), 045202.
[27] T. Feng, L. Lindsay, X. Ruan, Four-phonon scattering significantly reduces intrinsic thermal conductivity of solids, Phys. Rev. B 96 (2017) 161201.
[28] T. Feng, X. Ruan, Four-phonon scattering reduces intrinsic thermal conductivity of graphene and the contributions from flexural phonons, Phys. Rev. B 97 (2018), 045202.
[29] S. Hu, et al., Significant reduction in thermal conductivity of lithium cobalt oxide cathode upon charging: propagating and non-propagating thermal energy transport, ES Energy Environ. (2018) 7–12, https://doi.org/10.30919/esee8c140.
[30] H. Yang, et al., Highly anisotropic thermal transport in LiCoO 2, J. Phys. Chem. Lett. 10 (2019) 5552–5556.
[31] T. Feng, X. Ruan, Higher-order phonon scattering: advancing the quantum theory of phonon linewidth, thermal conductivity and thermal radiative properties, in: B. Liao (Ed.), Nanoscale Energy Transport, IOP Publishing, 2020, https://doi.org/10.1088/978-0-7503-1738-2ch2, 2-1-2–44.
[32] K. Takahata, I. Terasaki, Thermal conductivity of AxBO2 -type layered oxides Na0.77MnO2 and LiCoO2, Jpn. J. Appl. Phys. 41 (2002) 763–764.
[33] L. Wu, W.H. Lee, J. Zhang, First principles study on the electrochemical, thermal and mechanical properties of LiCoO2for thin film rechargeable battery, Mater. Today Proc. 1 (2014) 82–93.
[34] C. Delmas, C. Fouassier, P. Hagenmuller, Structural classification and properties of the layered oxides, Phys. B+C 99B (1980) 81–85.
[35] A. Jain, et al., Commentary: the Materials Project: a materials genome approach to accelerating materials innovation, Apl. Mater. 1 (2013), 011002.
[36] H. Kawaji, et al., Low temperature heat caoacity and thermodynamic functions of LiCoO2, J. Therm. Anal. Calorim. 68 (2002) 833–839.
[37] B. Taylor, H.J. Maris, C. Elbaum, Phonon focusing in solids, Phys. Rev. Lett. 23 (1969) 416–419.
[38] D.a. Broido, M. Malorny, G. Birner, N. Mingo, D.a. Stewart, Intrinsic lattice thermal conductivity of semiconductors from first principles, Appl. Phys. Lett. 91 (2007) 231922.
[39] T. Feng, X. Ruan, Prediction of spectral phonon mean free path and thermal conductivity with applications to thermoelectrics and thermal management: a review, J. Nanomater. (2014) 1–25, 2014.
[40] L. Lindsay, C. Hua, X.L. Ruan, S. Lee, Survey of ab initio phonon thermal transport, Mater. Today Phys. 7 (2018) 106–120.
[41] C.W. Li, et al., Orbitally driven giant phonon anharmonicity in SnSe: Supplement, Nat. Phys. 91 (2015) 1–8.
[42] M.D. Nielsen, V. Ozolins, J.P. Heremans, Lone pair electrons minimize lattice thermal conductivity, Energy Environ. Sci. 6 (2013) 570–578.
[43] J.U. Rahman, et al., Localized double phonon scattering and DOS induced thermoelectric enhancement of degenerate nonstoichiometric Li1-: XNbO2 compounds, RSC Adv. 7 (2017) 53255–53264.
[44] H. Wang, Y.I.I. Jang, B. Huang, D.R. Sadoway, Y.M. Chiang, TEM study of electrochemical cycling-induced damage and disorder in LiCoO 2 cathodes for rechargeable lithium batteries, J. Electrochem. Soc. 146 (1999) 473–480.
[45] N. Balke, et al., Nanoscale mapping of ion diffusion in a lithium-ion battery cathode, Nat. Nanotechnol. 5 (2010) 749–754.
[46] L. Wu, J. Zhang, Ab initio study of anisotropic mechanical properties of LiCoO2 during lithium intercalation and deintercalation process, J. Appl. Phys. 118 (2015) 1–7.
[47] F. Ning, S. Li, B. Xu, C. Ouyang, Strain tuned Li diffusion in LiCoO2 material for Li ion batteries: a first principles study, Solid State Ionics 263 (2014) 46–48.

[48] Y. Li, X. Cheng, Y. Zhang, First-principle analyses of stress and strain during Li deintercalation in LiCoO, ECS Trans. 19 (2009) 1–9.
[49] A. Moradabadi, P. Kaghazchi, J. Rohrer, K. Albe, Influence of elastic strain on the thermodynamics and kinetics of lithium vacancy in bulk LiCoO2, Phys. Rev. Mater. 1–9 (2018), 015402.
[50] J.C. Idrobo, et al., Temperature measurement by a nanoscale electron probe using energy gain and loss spectroscopy, Phys. Rev. Lett. 120 (2018), 095901.
[51] S. Mukhopadhyay, et al., Two-channel model for ultralow thermal conductivity of crystalline Tl3VSe4, Science 360 (80) (2018) 1455–1458.
[52] Y. Zhou, S. Xiong, X. Zhang, S. Volz, M. Hu, Thermal transport crossover from crystalline to partial- crystalline partial-liquid state, Nat. Commun. (2018) 1–28.

Dr. **Tianli Feng** is a Postdoctoral Research Associate at Oak Ridge National Laboratory (ORNL). He received his B.S. in Physics at the University of Science and Technology of China in 2011. He received his M.S. and Ph.D. in Mechanical Engineering at Purdue University in 2013 and 2017, respectively. While at ORNL from 2017 to 2019, he was also affiliated with Vanderbilt University. His research interests are in multiscale simulations and data sciences-enabled engineering of energy transport, conversion and storage.

Dr. **Andrew O'Hara** is a Postdoctoral Research Scholar at Vanderbilt University. He received his B.S. in Physics and Mathematics at Haverford College in 2009. He received his Ph. D. in Physics at The University of Texas at Austin in 2015. His research interests focus primarily on applications of density-functional theory to understand structural, electronic, and defect properties of oxides and various layered materials.

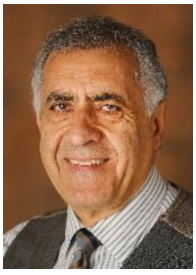

Sokrates T. Pantelides is University Distinguished Professor of Physics and Engineering, McMinn Professor of Physics, and Professor of Electrical Engineering at Vanderbilt University, Nashville, Tennessee, and Distinguished Visiting scientist at Oak Ridge National Laboratory. Ph.D. Physics, University of Illinois at Urbana-Champaign; researcher and research manager at IBM T.J. Watson Research Center in New York (1975–1994). Authored/coauthored ~700 papers with ~28,000 citations, edited nine books. Fellow of APS, MRS, AAAS, and IEEE. Theoretical/computational research on the structure, defect dynamics, and electronic/magnetic/electromechanical properties of materials and nanostructures, complex oxides, microscopy, two-dimensional materials, radiation effects, device physics and reliability, and catalysis.